Sensors & Diagnostics

PAPER

View Article Online
View Journal | View Issue

Cite this: *Sens. Diagn.*, 2025, **4**, 1014

Development of a broadly adaptable TR-FRET serological assay for sensitive and specific detection of infectious disease antibodies in human sera

Walaa A. Bedewy, [ab] Claudia C. dos Santos, [cd] Marc J. Adler, [a] Guennadi Saiko [ef] and Dustin J. Little *[a]

Detecting antibodies (Abs) is essential for assessing acquired immunity to infectious diseases, particularly following vaccination or prior infection. However, conventional serological tests often suffer from several limitations, including labor-intensive preparation, the need for specialized biosafety facilities, and lengthy processing times. Moreover, they provide only qualitative results with limited specificity. While homogeneous serological assays offer a simpler approach to detect Abs in biological samples, their sensitivity is often compromised by high background interference. In this study, we present a time-resolved fluorescence energy transfer (TR-FRET) assay for detecting infectious disease Abs in human sera. Our assay demonstrates high sensitivity in distinguishing between an antigen and its specific antibody, with no detectable upper limit of detection or prozone effect. It is universally applicable to various antigen–antibody complexes including SARS-CoV-2 and influenza, delivers accurate results within 15 minutes, and effectively mitigates background noise from human specimens. The development of this highly accurate immunoassay will enhance serological testing, making it faster, more reliable, and suitable for point-of-care settings.

Received 20th June 2025,
Accepted 28th August 2025

DOI: 10.1039/d5sd00102a

rsc.li/sensors

Introduction

Serological tests have been developed to identify antibodies (Abs) in human fluids, offering insights into an individual's disease history and assessing their level of acquired immunity. Moreover, serological tests have gained significant attention in recent years mainly in part due to the COVID-19 pandemic, as there was a heightened need to detect Abs against severe acute respiratory syndrome coronavirus 2 (SARS-CoV-2). Antibody detection for SARS-CoV-2 was essential for diagnosing infections, tracking close contacts, and monitoring immunity at both local and national levels for epidemiological and vaccine efficacy studies.[1,2]

Various immunoassays have been used for serological testing and the detection of SARS-CoV-2 Abs in serum. The plaque reduction neutralization test (PRNT) was considered the gold standard for detecting neutralizing Abs (nAbs) during the pandemic.[3] However, PRNT is slow, requires live virus, and must be conducted in biosafety level III facilities.[4] Alternatively, enzyme-linked immunosorbent assays (ELISAs) and lateral flow immunoassays (LFIAs) are among the most commonly used methods for serological testing. ELISA is quantitative and offers high accuracy and sensitivity.[5,6] However, it has major drawbacks including a long processing time, and requires lab infrastructure and personnel to prepare, process, and read the ELISA plates. On the other hand, LFIAs are rapid and simple which facilitate their point-of-care (POC) use, but they are qualitative, can have low specificity, and their sensitivity varies among different products.[7–9] Therefore, the need for a rapid, sensitive, quantitative, and homogeneous immunoassay is essential for reliable on-site testing and the effective development of vaccines against infectious diseases. Moreover, simplifying and making serological tests faster can pave the road to point-of-care testing (POCT), which may significantly improve outcomes by enabling clinical decisions during patient contact. To accomplish this, the test should be simple to

[a] *Department of Chemistry and Biology, Toronto Metropolitan University, Toronto, ON M5B 2K3, Canada. E-mail: djlittle@torontomu.ca*
[b] *Department of Pharmaceutical Chemistry, Faculty of Pharmacy, Helwan University, Egypt*
[c] *Keenan Research Centre for Biomedical Science at St. Michael's Hospital, Toronto, ON M5B 1T8, Canada*
[d] *Institute of Medical Science, University of Toronto, Toronto, ON M5S 3H2, Canada*
[e] *Department of Physics, Toronto Metropolitan University, Toronto, ON M5B 2K3, Canada*
[f] *Oxilight Inc., Toronto, ON, Canada*

perform in a POC environment, results available within 15 minutes, and have quantifiable capabilities. Only a limited number of homogeneous serological assays for the detection of Abs against infectious diseases have been developed. An example is a homogeneous immunoassay that employs a split-luciferase system.[10] However providing reliable results with high correlation to ELISA, it requires genetic engineering to incorporate peptide tags for generating luciferase luminescence. Additionally, fluorescence polarization (FP) can also be used for a homogeneous immunoassay, which has been used to detect SARS-CoV-2 Abs.[11] Although simple, the short-lived fluorophores used in FP suffer low signal-to-noise ratio due to the high background fluorescence created by plastic, reagents, or biological matrices that compromise assay sensitivity. One possible method to overcome these limitations is an immunoassay using fluorescence resonance energy transfer (FRET). FRET is a distance-sensitive technique in which non-radiative energy is transferred from an excited fluorophore, referred to as the "donor", to another fluorophore, the "acceptor", through long-range dipole–dipole interactions.[12,13] This energy transfer occurs over a range of 10–100 Å. The efficiency of transfer is inversely proportional to the sixth power of the distance between the donor and acceptor, as described by eqn (1).[14]

$$E = 1/(1 + R^6/R_0^6) \quad (1)$$

R is the distance between donor and acceptor and R_0 is Förster distance, the distance at which the efficiency of energy transfer is 50%.

The Förster distance primarily depends on three factors: the relative orientation of donor and acceptor fluorophores, the quantum yield of the donor, and the spectral overlap between the donor emission and the acceptor excitation wavelengths. For effective energy transfer, a spectral overlap of more than 30% is required.[15] Despite the advantages, FRET has several drawbacks: a) crosstalk, where the excitation light excites the acceptor instead of the donor, leading to emission that is not due to energy transfer; b) bleed-through, where the overlapping emission spectra of the donor and acceptor enhance the acceptor's emission; and c) background noise generated by biomolecules and plastics.[16] These issues can be mitigated by time-resolved fluorescence resonance energy transfer (TR-FRET).[17,18] TR-FRET utilizes lanthanides – rare earth elements – such as europium (Eu) and terbium (Tb) as "donor" and a fluorophore such as fluorescein, Cy5 or Alexa Fluor as a complementary acceptor.[19] Lanthanides are excited through an "antenna" in a process called sensitization. The antenna is a conjugated ligand with an excitation state higher than that of the lanthanide (Fig. 1a), which absorbs the incident light and transfers the energy to the lanthanide ion.[16,20] This creates a significant difference between the excitation wavelength absorbed by the ligand and the emission wavelength emitted by the lanthanide, thus overcoming crosstalk. The emission band of the lanthanide ion is narrow and sharp, significantly reducing bleed-through. Additionally, lanthanides have long lifetimes (μs–ms), which delays the emission of the acceptor after energy transfer, making it much longer than the background autofluorescence (ns).[21] TR-FRET has been employed for detecting protein–protein interactions (PPIs) utilizing lanthanides as donors with complementary acceptors.[22] When protein partners bind, the donor lanthanide and acceptor fluorophore come into close proximity, enabling energy transfer and generating a detectable TR-FRET signal. This method has been employed previously to screen inhibitors of PPIs in living cells using green fluorescent protein (GFP) and red fluorescent protein (RFP)-tagged proteins as donor and acceptor tags, respectively.[23]

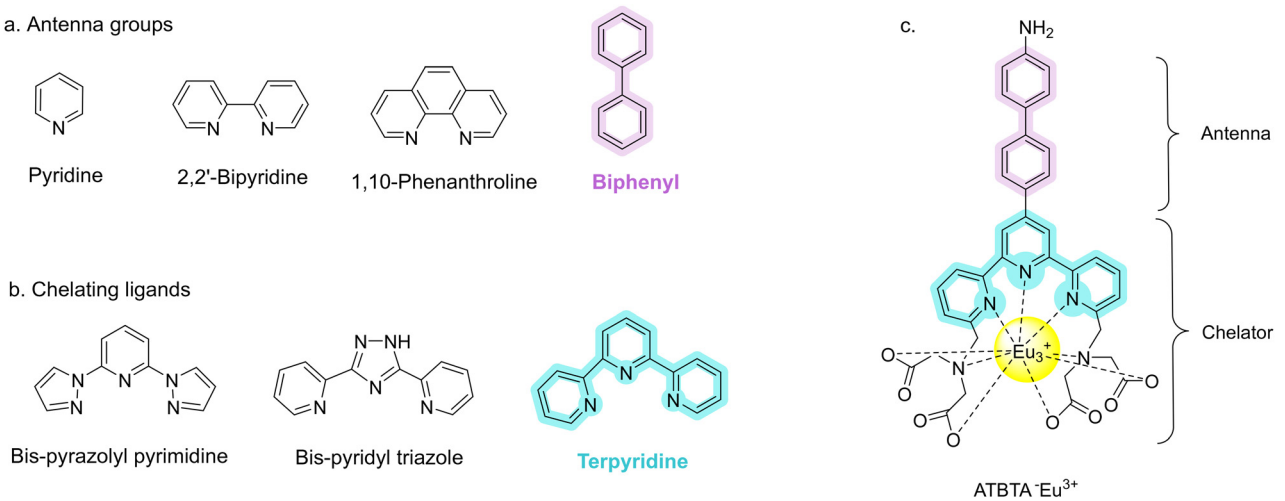

Fig. 1 Chemical structures of antenna groups and chelating ligands for lanthanide-based labeling. a) Examples of π-conjugated (hetero)aromatic moieties functioning as antennas. Notably, pyridine, 2,2-bipyridine and 1,10-phenanthroline also function as chelators. b) Examples of polydentate ligands used as chelators. c) Structure of Eu(III) complex (ATBTA-Eu^{3+}) featuring a biphenyl antenna, with the Eu^{3+} stabilized by nine coordination bonds with terpyridine ligand and polycarboxylate side chain.

In this study, we developed a homogeneous immunoassay for the serological detection of SARS-CoV-2 specific IgG immunoglobulins in human serum. The assay leverages a TR-FRET-based approach whereby immunoglobulins bound to a europium-labelled antigen are detected through FRET with recruitment of protein G fused to a fluorescent acceptor. The robustness of our TR-FRET assay is demonstrated by detecting Abs against SARS-CoV-2 in serum samples from immunized individuals and convalescent patients. Furthermore, we demonstrate the universality of the TR-FRET immunoassay by modifying the assay to work with europium-labelled influenza A hemagglutinin (HA) of the H7N9 strain and detection with monoclonal antibodies (mAbs).

Results and discussion

Immunoassay design

In order to design a robust TR-FRET-based assay, the choice of the donor and its complementary acceptor needed to be carefully considered as the excitation and emission spectra require sufficient separation to allow independent measurement of each fluorophore emission. Several lanthanide complexes, particularly Tb^{3+} and Eu^{3+}, are commercially available in various chelated forms. Optimal lanthanide chelates should exhibit high stability in aqueous media, good solubility, and a high quantum yield.[24,25] Polydentate ligands such as bis-pyrazolyl pyrimidine, bis-pyridyl triazole, and terpyridine are examples of multivalent ligands that form stable chelates with lanthanides (Fig. 1b).[26] Terpyridine (2,2′:6′,2″-terpyridine) is a tridentate ligand, coordinating the lanthanide ion through three pyridyl nitrogens.[27] The europium(III) complex, {2,2′,2″,2‴-{[4′-(aminobiphenyl-4-yl)-2,2′:6′,2″-terpyridine-6,6″-diyl]bis(methylenenitrilo)} tetrakis(acetato)} europium(III) (ATBTA-Eu^{3+}), incorporates a terpyridine ligand alongside four polycarboxylate chains at the 6,6′-positions of the terpyridine scaffold. This coordinates the central Eu^{3+} ion in a nonadentate structure (Fig. 1c), significantly enhancing the complex's stability and photoluminescence.[28] Thus, we utilized ATBTA-Eu^{3+} as the donor, which has an excitation and emission maxima at 340 nm and 615 nm, respectively. However, we needed to convert it to DTBTA-Eu^{3+} ({2,2′,2″,2‴-{[4′-(3,5-dichloro-2,4,6-triazin-aminobiphenyl-4-yl)-2,2′:6′,2″-terpyridine-6,6″-diyl]bis(methylenenitrilo)}tetrakis-(acetato)} europium(III)) before conjugating it to a protein of interest (Scheme S1). Alexa Fluor 647 was selected as the acceptor, which exhibits excitation and emission maxima at 615 nm and 671 nm, respectively. Representative excitation and emission scans of DTBTA-Eu^{3+} and Alexa Fluor 647 conjugated to protein carriers are shown in Fig. S1. Next, we needed to define optimal reagents for detection of Abs in a sample. The spike glycoprotein is a large surface antigen displayed on the surface of SARS-CoV-2 and is a critical component for viral infectivity. More specifically, the region of the spike protein important for engaging host cells is called the receptor binding domain (RBD), which interacts with the host receptor angiotensin converting enzyme 2 (ACE2).[29] Interestingly, more than 90% of nAbs in serum are specific to the spike RBD as it disrupts binding to ACE2,[30] which makes it an ideal choice for detecting humoral immunity levels. The second aspect for the assay requires an acceptor molecule to be close in proximity to the donor. In this case we chose protein G labelled with Alexa Fluor 647 as the acceptor reagent. Protein G has a high binding affinity for the Fc region of IgG but not for IgM, IgA, or IgE.[31–33] However, only protein G-Alexa Fluor 647 bound to spike RBD IgG will be close enough to facilitate energy transfer from Eu^{3+}-DTBTA, enabling detection.

Eu^{3+}-DTBTA labeling of Spike RBD (319–591)

Spike RBD containing residues 319–591 (referred to as RBD hereafter) was cloned into pcDNA3.1 with an N-terminal synthetic endoplasmic reticulum targeting peptide and a C-terminal poly-lysine (polyLys) tag followed by a tobacco etch virus (TEV) cleavable octa-histidine tag, as outlined in the SI. A polyLys tag was engineered into the C-terminus of the RBD protein to enhance labeling at a site that is as distal from the ACE2 and known anti-spike antibody binding sites. This ensured that there would be minimal, if any, perturbations to the structure or function of RBD. This form of the RBD was transfected into Expi293 cells, purified, and labeled with Eu^{3+}-DTBTA via nucleophilic substitution, after cyanuric chloride-mediated activation of the antenna's aromatic amine (Scheme S1).

Unlike organic fluorophores with short lifetimes, lanthanide luminescence is not subject to concentration quenching, making multiple labeling advantageous for enhancing signal intensity.[26] The labeling efficiency was calculated as shown for eqn (2) below:

$$\frac{\text{molar concentration at 335 nm}}{\text{molar concentration at 595 nm}} \times 100 \quad (2)$$

The molar concentration of Eu-labeled RBD at λ = 335 nm was calculated using molar absorptivity 31 000 cm^{-1} M^{-1}, as cited previously for Eu^{3+}-ATBTA.[28] The molar concentration of RBD was determined using the Bradford assay at λ = 595 nm. To assess how labeling efficiency affects RBD binding to anti-spike Abs, we prepared RBD with different labeling levels (105% and 440%). The variation in labeling did not appear to impact Eu^{3+}-DTBTA labeled RBD (Eu-RBD) binding to anti-spike Abs (Fig. S2), and thus we utilized the Eu-RBD with 440% labeling efficiency moving forward.

Immobilized ACE2 can capture Eu-RBD

Next, we wanted to test the functionality of the Eu-RBD, as this modification could impair the RBD interaction with ACE2. To do this we conducted a modified version of an ELISA, but using immobilized ACE2 and direct

luminescence read-out of Eu-RBD. ACE2 (0.5 μg) was immobilized on high-binding 96-well black plates, the wells were blocked, and then were incubated with serial dilutions of Eu-RBD (starting at 20 μg mL^{-1}) for 1 hour. The plate was then washed, and time-resolved fluorescence (TRF) intensity of the wells was then measured to determine the levels of ACE2-dependent captured of Eu-RBD. As seen in Fig. 2, the fluorescence intensity increased exponentially with increasing concentrations of Eu-RBD, which represents increased captured by ACE2. Whereas, a negative control consisting of a well without ACE2, showed no significant signal. Together, this indicates that europium labeling of RBD does not interfere with the binding to ACE2.

Optimization of assay reagents and parameters

Optimizing the concentration of Eu-RBD. To optimize the optimal concentration of Eu-RBD in the TR-FRET immunoassay, we leveraged the use of anti-spike (1-3A7) and anti-nucleocapsid (R019) mAbs as positive and negative controls, respectively. Eu-RBD was prepared at a starting concentration of 500 nM and serially diluted to 0.97 nM. A mixture of anti-spike (1-3A7) or anti-nucleocapsid (R019) mAbs premixed with protein G-Alexa Fluor 647 at equimolar concentration (10 nM) were then added to the plate, incubated for 15 minutes and recorded. The plate was read at excitation wavelength 340 nm for europium, and emission wavelengths of 615 nm for Eu^{3+}-DTBTA, and 665 nm for Alexa Fluor 647. The TR-FRET ratio was calculated as show in eqn (3) below:

$$\text{signal intensity at 665 nm/signal intensity at 615 nm} \quad (3)$$

Eu-RBD incubated with anti-spike mAb showed a signal (TR-FRET ratio) increase within the Eu-RBD concentration range of 0.97–31 nM, followed by a gradual decrease from 31–62 nM, and a sharp drop beyond 62 nM (Fig. S3a). This decline is attributed to the prozone effect,[34] where the concentration of Eu-RBD exceeds the mAb saturation point. In contrast, no signal change was observed when Eu-RBD was incubated with the SARS-CoV-2 anti-nucleocapsid mAb (Fig. S3a). Next, we wanted to identify the optimal Eu-RBD concentration within the 1–60 nM range that provides the highest detection sensitivity. To do this, we assayed Eu-RBD at concentrations of 1, 10, and 60 nM, which were then combined with serially diluted anti-spike mAb and protein G-Alexa Fluor 647, starting at an equimolar concentration of 250 nM. The 1 nM and 10 nM Eu-RBD produced similar signals (TR-FRET ratio), which were slightly better than the 60 nM concentration at lower anti-spike mAb concentrations (8–100 nM) (Fig. S3b). Based on these results, 1 nM Eu-RBD was selected as the optimal concentration for further experiments.

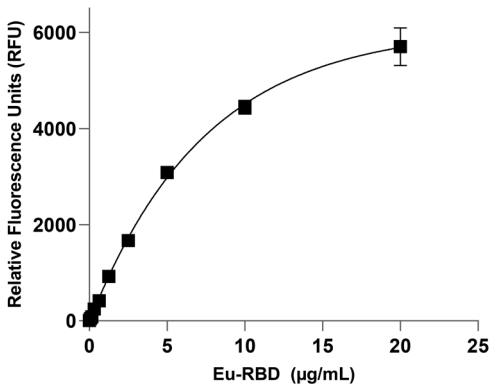

Fig. 2 ACE2 effectively captures Eu-RBD. ACE2 was immobilized in a 96-well high binding black plate at 0.5 μg overnight at 4 °C. Afterwards, serially diluted Eu-RBD starting at 20 μg mL^{-1} was then added to the plate. After 1 hour incubation and extensive washings, TRF intensity of captured Eu-RBD was measured at excitation and emission wavelengths, 340 nm and 615 nm, respectively. Data points represent the mean of three independent replicates (n = 3) and error bars are standard deviation (SD).

Optimizing concentration of Alexa Fluor 647 labeled-protein G. To study the effect of varying the concentration of protein G-Alexa Fluor 647 relative to mAbs, protein G-Alexa Fluor 647 at 10 nM or 100 nM was premixed with constant anti-spike mAb (1-3A7, 100 nM), and the mixture was serially diluted. Eu-RBD was then added at a constant concentration of 1 nM, as determined earlier. At 10 nM protein G-Alexa Fluor 647, which is a 10-fold lower concentration relative to the anti-spike mAb, the signal began to decrease at higher concentration of mAb (25 nM) (Fig. S3c). This indicates that equimolar concentrations of anti-spike mAb and protein G-Alexa Fluor 647 are necessary to generate a reliable TR-FRET signal. Thus, we chose to use 100 nM G-Alexa Fluor 647 and 1 nM Eu-RBD moving forward with the assay.

Effect of temperature and time on immunoassay performance. In addition to reagent concentration and ratios, we also wanted to test the effect of temperature and time on assay performance. First, the binding of anti-spike mAb (3-6B1) and anti-nucleocapsid mAb (R019) to Eu-RBD was tested at room temperature and 37 °C. Equimolar concentrations of mAb and protein G-Alexa Fluor 647 (100 nM) were serially diluted in wells, followed by the addition of 1 nM Eu-RBD. Plates were incubated for 15 minutes at either room temperature or 37 °C. The signal increase for the anti-spike mAb (3-6B1) at 37 °C exhibited a linear increase, likely due to the accelerated equilibrium reached at lower mAb concentrations as a result of the elevated incubation temperature (Fig. S4a). On the other hand, the anti-nucleocapsid mAb (R019) did not show a significant signal increase under either condition (Fig. S4a). Thus, we moved forward with room temperature as the immunoassay incubation condition. Next, we tested immunoassay incubation time by premixing equimolar concentrations (100 nM) of protein G-Alexa Fluor 647 with anti-spike mAbs (3-6B1 and 1-3A7) and anti-nucleocapsid mAb (R019), separately, and added in Eu-RBD (1 nM) then incubated the plate at different time intervals (5, 15, and 120 minutes). For the anti-spike mAb 3-6B1, binding equilibrium was

achieved within 5 minutes, as the binding signal (TR-FRET ratio) was similar to that observed after 15 minutes of incubation (Fig. S4b). In contrast, the anti-spike mAb 1-3A7 reached equilibrium at 15 minutes (Fig. S4c), suggesting that the time required for equilibrium likely correlates with binding affinity or location of anti-spike Abs with RBD. Lastly, after 2 hours of incubation, both 3-6B1 and 1-3A7 showed a linear increase in signal due to enhanced detection of lower mAb concentrations with prolonged incubation (Fig. S4b and c), while the varied incubation times had no effect on the binding of the anti-nucleocapsid mAb (R019).

The TR-FRET immunoassay using Eu-RBD is specific for anti-spike antibodies

Now that we had optimized TR-FRET immunoassay conditions, we wanted to test the specificity of the assay by evaluating the binding of Eu-RBD to various anti-spike and anti-nucleocapsid mAbs. Each mAb, starting at a concentration of 100 nM, was individually premixed with protein G-Alexa Fluor 647 (100 nM) and serially diluted in a 384-well white plate. Eu-RBD was then added at 1 nM to all wells, and the plate was incubated for 15 minutes at room temperature (Fig. 3a). Among the anti-spike mAbs, 3-6B1 showed a ~3-fold increase in the TR-FRET signal, while 1-3A7 and D003 exhibited ~2.8-fold increases (Fig. 3b). The lowest signal was observed with MM57, which showed a ~1.5-fold increase at a concentration of 100 nM. The variation in FRET signals among different anti-spike mAbs likely reflects binding to distinct motifs on the RBD, influencing the relative orientation and energy transfer efficiency between the Eu^{3+} "donor" and Alexa Fluor 647 "acceptor". Despite these differences between anti-spike mAbs, the assay conducted with anti-nucleocapsid mAbs showed negligible increases in the FRET signal (Fig. 3b), highlighting a high degree of specificity in our immunoassay. Notably, none of the mAbs exhibited a prozone effect, even at high concentrations.

Testing serum samples from immunized individuals with known concentrations of anti-spike antibodies

As our immunoassay showed excellent performance with standard mAb samples, we wanted to test if it performed equally as well using real biological serum samples. To do this we utilized ten serum samples from vaccinated individuals obtained from BEI resources, whereby the individuals received different combinations of vaccine manufacturers, and their anti-spike antibody levels were determined. Pre-mixed Eu-RBD and protein G-Alexa Fluor 647 were added to the diluted serum, followed by a 15 minute incubation (Fig. 4a), facilitating a simplified reagent addition protocol suitable for POC settings. Serum samples were tested at a 1 : 40 dilution and evaluated according to their reported anti-spike antibody titres from BEI resources, where anti-spike antibody concentrations correlate with the neutralization potential of ACE2–RBD binding.[35] The highest TR-FRET ratio (1.5) was observed for sample NRH-21761 (Fig. 4b), which had the highest anti-spike Abs concentration (9342 IU mL^{-1}). This was followed by NRH-21765 (7140 IU mL^{-1}) with TR-FRET ratio of 1.1. NRH-21740 (2572 IU mL^{-1}) and NRH-21747 (2253 IU mL^{-1}) exhibited comparable signals, both with a TR-FRET ratio of 0.7; while other samples, including NRH-21762 (2014 IU mL^{-1}), NRH-20012 (1936 IU mL^{-1}), NRH-17846 (1385 IU mL^{-1}), and NRH-17727 (1273 IU mL^{-1}), showed TR-FRET ratios ranging from 0.6 down to 0.4. The sample with the lowest anti-spike antibody concentration, NRH-21261 (605 IU mL^{-1}), exhibited the lowest TR-FRET ratio of 0.1. Despite the strong congruence of increased TR-FRET ratio to anti-spike antibody levels, sample NRH-21756 (2572 IU mL^{-1}) produced a signal that was inconsistent with its reported antibody concentration; showing higher TR-FRET ratio signal than other serum samples of similar reported concentration range of Abs (NRH-21740 & NRH-21747). This could be due to a higher propensity of anti-

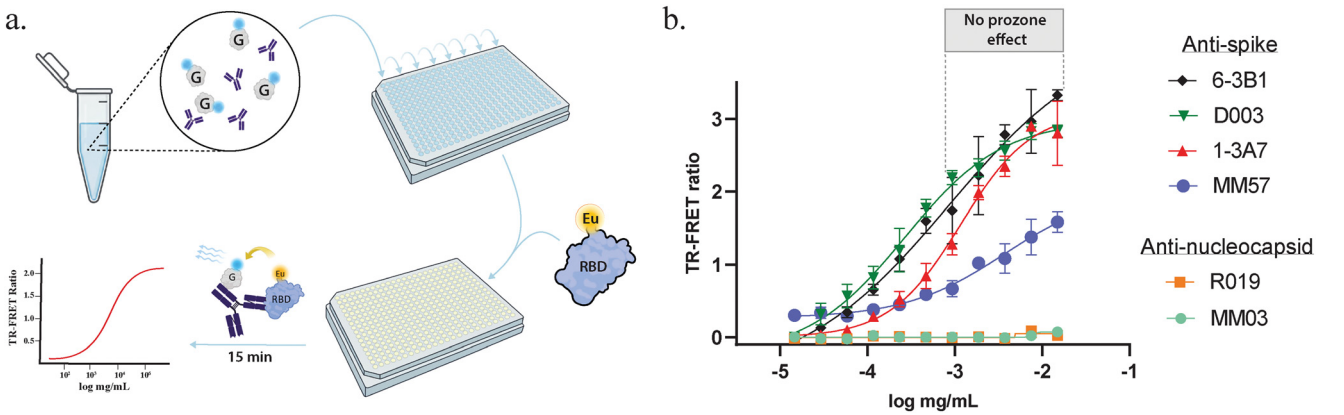

Fig. 3 Procedure and specificity of the TR-FRET immunoassay. a) Schematic illustration of the TR-FRET immunoassay of Eu-RBD with anti-spike mAbs. mAbs at starting concentration 0.015 mg mL^{-1} were premixed, separately, with 100 nM G-Alexa Fluor 647 and serially diluted in 384-well plate. Eu-RBD was added at 1 nM and the plate was incubated for 15 minutes. b) Concentration-dependent FRET signal increase of different anti-spike (6-3B1, D003, 1-3A7, and MM57) and anti-nucleocapsid (R019 and MM03) mAbs. Concentrations are final concentrations in wells. Data points represent the mean of three independent replicates (n = 3) and error bars are SD.

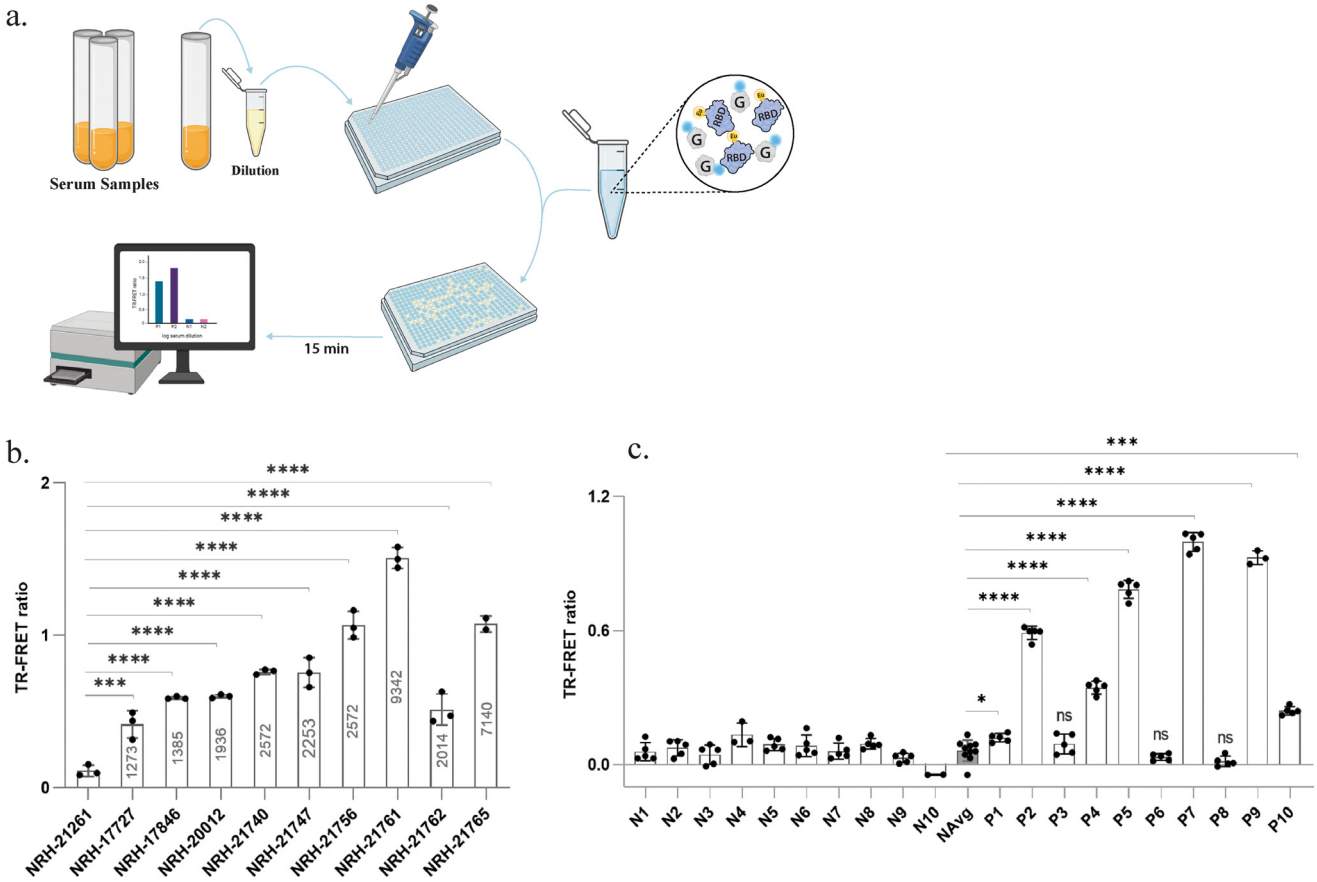

Fig. 4 The TR-FRET ratio correlates with anti-spike antibody levels in a sample. a) Schematic illustration of testing human sera utilizing the TR-FRET immunoassay; serum was dispensed in 384-well plate at 1 : 40 dilution, then mixture of protein G-Alexa Fluor 647 (100 nM) and Eu-RBD (1 nM) was added, and the plate was read after 15 minute incubation. b) TR-FRET of immunized serum samples; n = 3 for all samples except NRH-21765 (n = 2). Numbers in bars indicate anti-spike antibody concentrations (IU mL^{-1}). Serum sample NRH-21261 with the lowest concentration of anti-spike antibodies (605 IU mL^{-1}) served as the reference sample for significance testing. c) Serum samples tested as positive (P1–P10) and negative (N1–N10) to COVID-19; n = 5 for all serum samples except N4, P9 (n = 3) and N10 (n = 2). NAvg represents the mean of serum samples N1–N10 and was used as the negative control for significance testing of positive serum samples. All data were normalized by subtracting the TR-FRET ratio of the blank represented as the zero line. Concentrations are final concentrations in wells. Bar graphs represent the mean from independent replicates and error bars are SD. Statistics performed by one-way ANOVA, *$p < 0.05$, ***$p < 0.001$, ****$p < 0.0001$, ns = not significant.

spike Abs that bind a specific epitope on RBD that allows for a more robust or sustained FRET (*i.e.* closer proximity). In fact, we would expect there to be some outliers as individual immune responses can be biased towards certain antigen epitopes. This has been previously observed in COVID-19 patients displaying altered antibody epitope mapping on spike glycoprotein depending on disease severity.[36] Moreover, our results are congruent with a previous study testing the same immunized serum samples using a semi-quantitative LFIA. Mahmud *et al.* showed that serum samples NRH-21740, -21747, -21756, -21761, and -21765 could completely neutralize RBD binding to ACE2 on a lateral flow paper fluidic substrate.[37]

Testing serum samples from healthy or convalescent individuals with unknown concentrations of anti-spike antibodies

Now that we established the validity of our TR-FRET immunoassay using serum samples from immunized individuals, we wanted to further test its applicability to COVID-19 positive patients. For this we utilized our same optimized immunoassay conditions, but with serum samples collected from patients testing positive for SARS-CoV-2 at the beginning of the COVID-19 pandemic (March 2020), or from healthy individuals before the pandemic. Each serum sample was diluted at 1 : 40 into the assay reaction and the TR-FRET ratio was determined (Fig. 4c). This reflects the relative concentration of RBD-specific Abs in each sample, varied across the samples, where the blank sample containing Eu-RBD and protein G-Alexa Fluor 647 (with no serum) represents the zero line. COVID-19 positive samples P2, P5, P9, and P7 exhibited the highest TR-FRET ratio signals of 0.6, 0.7, 0.8, and 1.0, respectively, indicating relatively high anti-spike antibody concentrations. Whereas COVID-19 positive sample P4 showed a moderate signal of 0.3. Furthermore, lower signals were observed for COVID-19 positive samples P1, P3, and P10 (TR-FRET ratios of 0.1) and P6 (0.03). Sample P8 exhibited a poor signal, suggesting a scarcity of anti-spike Abs. The variations in TR-FRET signal among COVID-19

positive sera are likely influenced by multiple factors affecting antibody production during and after infection. These factors may include individual differences such as age, underlying chronic diseases, use of immunosuppressants or glucocorticoids, and the severity or duration of infection.[38–40] Our findings are highly correlated with the results of testing the exact same convalescent patient serum samples using the semi-quantitative LFIA with immobilized ACE2 by Mahmud *et al.* where samples P2, P4, P5, P7, P9, and P10 were able to completely neutralize ACE2 capture of RBD on a paper fluidic substrate. As shown in Fig. 4c, we also observed the strongest TR-FRET ratio with samples P2, P4, P5, P7, and P9. Moreover, P8 showed the lowest signal in the TR-FRET immunoassay, which also was the lowest anti-spike antibody containing serum sample observed in the semi-quantitative LFIA.[37] Further supporting the specificity of our TR-FRET assay, serum from healthy individuals, samples N1–10, showed little to no TR-FRET ratio in line with the fact they had not been exposed to SARS-CoV-2.

Assessing the upper detection limit of the TR-FRET immunoassay

To evaluate the upper detection limit and test the prozone effect at higher concentrations, we serially diluted the anti-spike mAb (6-3B1), starting at 0.5 mg mL^{-1} (which covers the typical prozone effect range), after premixing it with 100 nM protein G-Alexa Fluor 647. We then added 1 nM Eu-RBD and incubated the plate for 1 hour. The TR-FRET ratio exhibited a slight increase, indicating that the assay had reached the plateau phase without displaying a prozone effect (Fig. 5a). To determine the upper limit of detection for anti-spike Abs in serum, we then selected two immunized serum samples with the highest antibody concentration (NRH-21761 and NRH-21765). Each serum sample was premixed separately with 100 nM protein G-Alexa Fluor 647, starting at 2000 IU mL^{-1}, serially diluted and incubated with 1 nM Eu-RBD for 1 hour. Both samples demonstrated a proportional increase in the TR-FRET ratio with increasing serum concentrations, without showing a prozone effect at high anti-spike antibody levels (Fig. 5b). In contrast, the TR-FRET assay developed by Yue *et al.* exhibited a prozone effect at high IgG concentrations, requiring a 1 : 150 serum dilution to prevent false negatives.[41] In their study, Yue *et al.* used secondary Abs for anti-spike antibody detection, with terbium as the "donor" and "BODIPY FL" as the acceptor. To determine whether the use of secondary Abs instead of protein G contributed to the prozone effect in their assay, we premixed NRH-21761 with 100 nM of either anti-human IgG Alexa Fluor 647 or protein G-Alexa Fluor 647 and then serially diluted the mixture without prior dilution. Afterwards, 1 nM Eu-RBD was added, and the mixture was incubated for 1 hour. The use of protein G-Alexa Fluor 647 generated a slightly stronger signal than anti-human IgG Alexa Fluor 647,

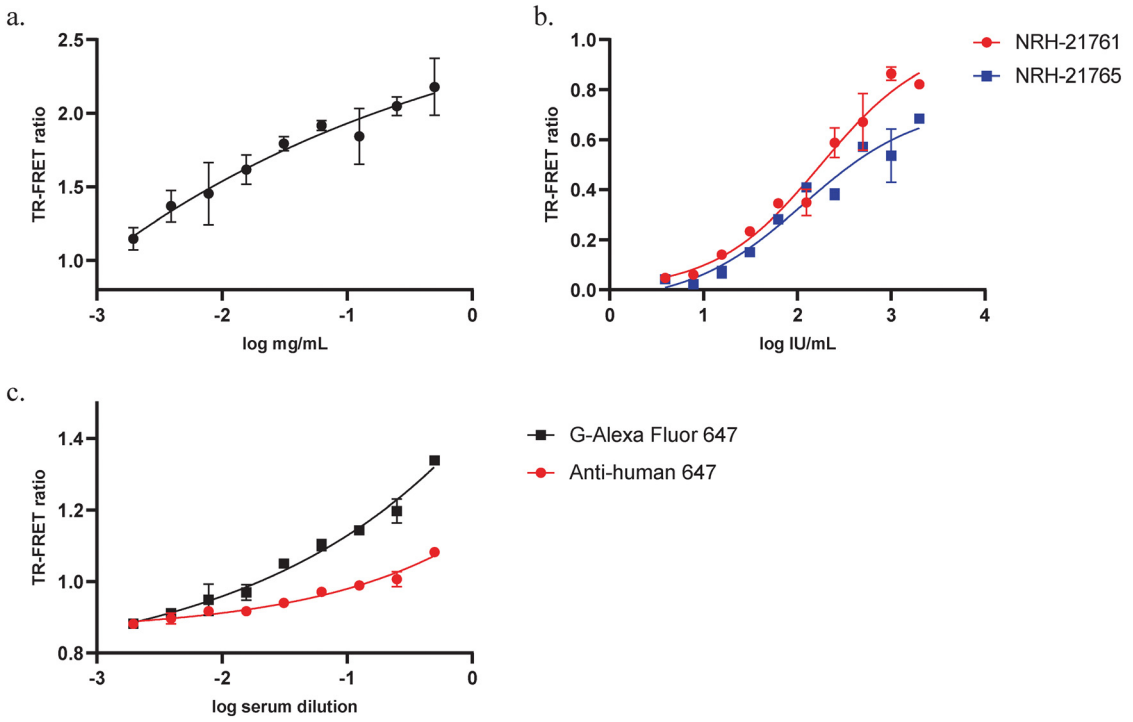

Fig. 5 The upper detection limit of the TR-FRET assay does not depend on anti-spike antibody concentration nor choice of IgG binding partner. a) Anti-spike 6-3B1 starting at 0.5 mg mL^{-1} (n = 3), b) immunized serum samples (NRH-21761 and NRH-21765) starting at 2000 IU mL^{-1} (n = 2), and c) NRH-21761 starting at 1 : 2 dilution (n = 2), were tested for upper detection limit. Protein G-Alexa Fluor 647 or anti-human IgG Alexa Fluor 647 was premixed with sample at 100 nM before serial dilution. Eu-RBD (1 nM) was added and the readings were recorded after 1 hour incubation. Data points represent the mean of independent replicates and error bars are SD.

particularly at high anti-spike antibody concentrations (Fig. 5c). However, in both cases, the signal did not decrease at high antibody levels. This suggests that the use of a secondary antibody did not impact the upper detection limit and that the false-negative signals observed in the assay from Yue *et al.* may have resulted from using a different donor–acceptor pair or other unidentified factors.

Evaluating the versatility of the developed TR-FRET assay across various antigen–antibody detection systems

Lastly, we wanted to test if our TR-FRET immunoassay principle could be extended to other viral pathogens that induce an immune response through a key viral antigen required for host attachment or viral infectivity. For this we chose influenza virus as a good candidate for expanding our assay as it uses hemagglutinin (HA) to attach to host cells, which is also the main source of immunity through vaccination. Thus, we obtained the HA protein of influenza A virus (H7N9) and labeled it with Eu^{3+}-DTBTA just as we did with RBD, with an efficiency of 182%. Europium labeled HA (Eu-HA) was then tested against two mAbs specific for H7N9 (NR-51191 and NR-51193) and one mAb not specific for H7N9 but rather for H5N1 (NR-15697). Each mAb was premixed separately with protein G-Alexa Fluor 647 at equimolar concentration and serially diluted. Afterwards, Eu-HA was added at a constant concentration of 1 nM, incubated, and analyzed. The immunoassay showed a representative increase in TR-FRET ratio with increasing amount of H7N9-specific Abs. NR-51193 showed higher levels than NR-51191 (Fig. 6). These differences could be based on multiple factors, such as binding to different HA epitopes, which affects the relative orientation and energy transfer efficiency between the Eu^{3+} "donor" and Alexa Fluor 647 "acceptor". Alternatively, it could be attributed to variations in the binding affinity of the two mAbs to HA. Despite these differences, the mAb specific for HA from H5N1 strain showed little to no increase in TR-FRET ratio (Fig. 6), further supporting that the immunoassay for Eu-HA also has high specificity.

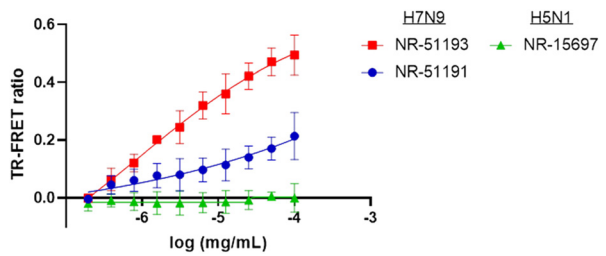

Fig. 6 TR-FRET assay of Eu-labeled hemagglutinin (HA) from influenza A (H7N9) with anti-HA specific for H7N9 (NR-51191 and NR-51193) or H5N1 (NR-15697). Anti-HA mAbs were premixed with 100 nM protein G-Alexa Fluor 647 and serially diluted starting at 100 nM (0.015 mg mL^{-1}). Eu-HA was added at 1 nM and the plate was incubated for 15 minutes before reading. Data points represent the mean of three independent replicates (n = 3) and error bars are SD.

Conclusions

Herein, we have developed a robust homogeneous serological assay for the specific detection of infectious disease Abs in human sera. Our TR-FRET assay utilizes the lanthanide europium (Eu) for its time-resolved luminescence properties, which help minimize background noise from biological specimens, enhancing detection sensitivity. To achieve this, we labeled the target antigens spike RBD and influenza A (H7N9) hemagglutinin with Eu. These labeled antigens were used to detect their corresponding Abs. Additionally, we employed protein G conjugated to Alexa Fluor 647, which binds to the Fc region of IgG. Given that FRET efficiency is distance-dependent, only protein G-Alexa Fluor 647 bound to antigen-specific Abs receives energy transfer from Eu, ensuring highly specific detection. We validated the assay by detecting SARS-CoV-2 anti-spike Abs in human sera from both healthy individuals and COVID-19-positive patients. Furthermore, we assessed its sensitivity using sera from immunized individuals with known anti-spike antibody concentrations. Notably, the assay does not exhibit an upper detection limit or a prozone effect at high antibody levels, thereby preventing false negatives and provides robust results within 15 minutes. This simple but innovative TR-FRET assay enhances serological testing by providing a faster, more reliable, and widely accessible approach, that could ultimately improve immune monitoring, disease control strategies, and public health decision-making in the future.

Author contributions

Walaa A. Bedewy: conceptualization, methodology, validation, formal analysis, investigation, data curation, visualization, writing – original draft, writing – review & editing. Claudia C. dos Santos: resources. Marc J. Adler: conceptualization, validation, resources, visualization, writing – review & editing, supervision, project administration, funding acquisition. Guennadi Saiko: conceptualization, methodology, validation, resources, visualization, writing – review & editing, supervision, project administration, funding acquisition. Dustin J. Little: conceptualization, methodology, validation, formal analysis, investigation, resources, visualization, data curation, writing – original draft, writing – review & editing, supervision, project administration, funding acquisition.

Conflicts of interest

The authors declare no conflicts of interest.

Data availability

Supplementary information: Experimental procedures, biological strains, plasmids, oligonucleotide primers, and additional data figures are provided as SI. Data for this article in reference to immunized serum samples in Fig. 4 and 5 are available from BEI resources (**https://www.beiresources.org/**). Data collected from human participants donating serum

samples used in Fig. 4 are not available due to confidentiality reasons. See DOI: https://doi.org/10.1039/D5SD00102A.

All experiments performed were approved by and in compliance with the St. Michaels Hospital and Toronto Metropolitan University ethics board (REB# 20-078 and REB# 2021-239, respectively). Informed consents were obtained from human participants of this study.

Acknowledgements

This research has been supported by Mitacs through the Mitacs Accelerate program (IT35998) to D. J. L., M. J. A., G. S., and W. A. B.; the Canadian Institutes of Health Research (CIHR, FRN 173206 and 175501) in partnership with the Public Health Agency of Canada (PHAC) and in collaboration with the COVID-19 Immunity Task Force (CITF) to D. J. L.; the Canadian Foundation for Innovation (CFI, 39773), Ontario Research Fund (ORF, 39733), the Toronto Metropolitan University Faculty of Science Dean's Research Fund and OVPRI internal equipment grant to D. J. L.; and the Toronto Metropolitan University Analysis Grant to G. S.

We would like to acknowledge the contribution of BEI Resources for providing us antibodies (monoclonal anti-RBD, anti-nucleocapsid, and anti-HA antibodies), and pooled serum samples with a known concentration of anti-spike antibody (IU mL^{-1}). We would like to thank Drs. Darius Rackus, Scott Tsai, and Michael Olson for use of reagents, facilities, and infrastructure for this project. We would like to thank the research coordinators that collected human samples, and the patients and families that generously consented to participate in research.

Notes and references

1 A. T. Huang, B. Garcia-Carreras, M. D. T. Hitchings, B. Yang, L. C. Katzelnick, S. M. Rattigan, B. A. Borgert, C. A. Moreno, B. D. Solomon, L. Trimmer-Smith, V. Etienne, I. Rodriguez-Barraquer, J. Lessler, H. Salje, D. S. Burke, A. Wesolowski and D. A. T. Cummings, *Nat. Commun.*, 2020, **11**, 4704.

2 R. W. Peeling, C. J. Wedderburn, P. J. Garcia, D. Boeras, N. Fongwen, J. Nkengasong, A. Sall, A. Tanuri and D. L. Heymann, *Lancet Infect. Dis.*, 2020, **20**, e245–e249.

3 N. M. A. Okba, M. A. Müller, W. Li, C. Wang, C. H. GeurtsvanKessel, V. M. Corman, M. M. Lamers, R. S. Sikkema, E. de Bruin, F. D. Chandler, Y. Yazdanpanah, Q. Le Hingrat, D. Descamps, N. Houhou-Fidouh, C. B. E. M. Reusken, B.-J. Bosch, C. Drosten, M. P. G. Koopmans and B. L. Haagmans, *Emerging Infect. Dis.*, 2020, **26**, 1478–1488.

4 J. J. Wang, N. Zhang, S. A. Richardson and J. V. Wu, *Expert Rev. Mol. Diagn.*, 2021, **21**, 363–370.

5 F. Amanat, D. Stadlbauer, S. Strohmeier, T. H. O. Nguyen, V. Chromikova, M. McMahon, K. Jiang, G. A. Arunkumar, D. Jurczyszak, J. Polanco, M. Bermudez-Gonzalez, G. Kleiner, T. Aydillo, L. Miorin, D. S. Fierer, L. A. Lugo, E. M. Kojic, J. Stoever, S. T. H. Liu, C. Cunningham-Rundles, P. L. Felgner, T. Moran, A. García-Sastre, D. Caplivski, A. C. Cheng, K. Kedzierska, O. Vapalahti, J. M. Hepojoki, V. Simon and F. Krammer, *Nat. Med.*, 2020, **26**, 1033–1036.

6 M. Dogan, L. Kozhaya, L. Placek, C. Gunter, M. Yigit, R. Hardy, M. Plassmeyer, P. Coatney, K. Lillard, Z. Bukhari, M. Kleinberg, C. Hayes, M. Arditi, E. Klapper, N. Merin, B. T.-T. Liang, R. Gupta, O. Alpan and D. Unutmaz, *Commun. Biol.*, 2021, **4**, 129.

7 B. G. Andryukov, *AIMS Microbiol.*, 2020, **6**, 280–304.

8 X. Duan, Y. Shi, X. Zhang, X. Ge, R. Fan, J. Guo, Y. Li, G. Li, Y. Ding, R. A. Osman, W. Jiang, J. Sun, X. Luan and G. Zhang, *Biosens. Bioelectron.*, 2022, **199**, 113883.

9 M. Lisboa Bastos, G. Tavaziva, S. K. Abidi, J. R. Campbell, L.-P. Haraoui, J. C. Johnston, Z. Lan, S. Law, E. MacLean, A. Trajman, D. Menzies, A. Benedetti and F. Ahmad Khan, *BMJ*, 2020, m2516.

10 Z. Yao, L. Drecun, F. Aboualizadeh, S. J. Kim, Z. Li, H. Wood, E. J. Valcourt, K. Manguiat, S. Plenderleith, L. Yip, X. Li, Z. Zhong, F. Y. Yue, T. Closas, J. Snider, J. Tomic, S. J. Drews, M. A. Drebot, A. McGeer, M. Ostrowski, S. Mubareka, J. M. Rini, S. Owen and I. Stagljar, *Nat. Commun.*, 2021, **12**, 1806.

11 K. Nishiyama, K. Takahashi, M. Fukuyama, M. Kasuya, A. Imai, T. Usukura, N. Maishi, M. Maeki, A. Ishida, H. Tani, K. Hida, K. Shigemura, A. Hibara and M. Tokeshi, *Biosens. Bioelectron.*, 2021, **190**, 113414.

12 T. Foerster, DELOCALIZED EXCITATION AND EXCITATION TRANSFER. Bulletin No. 18, Oak Ridge, TN (United States), 1964.

13 R. S. Knox, *J. Biomed. Opt.*, 2012, **17**, 011003.

14 C. G. dos Remedios, M. Miki and J. A. Barden, *J. Muscle Res. Cell Motil.*, 1987, **8**, 97–117.

15 R. B. Sekar and A. Periasamy, *J. Cell Biol.*, 2003, **160**, 629–633.

16 S. Wheeler and S. J. Butler, *Analysis Sensing*, 2023, **3**, e202200036.

17 J.-C. G. Bünzli and C. Piguet, *Chem. Soc. Rev.*, 2005, **34**, 1048.

18 M. C. Heffern, L. M. Matosziuk and T. J. Meade, *Chem. Rev.*, 2014, **114**, 4496–4539.

19 F. Degorce, *Curr. Chem. Genomics*, 2009, **3**, 22–32.

20 E. G. Moore, A. P. S. Samuel and K. N. Raymond, *Acc. Chem. Res.*, 2009, **42**, 542–552.

21 P. Manna, M. Bhar and P. Mukherjee, *J. Lumin.*, 2021, **235**, 118052.

22 W. Lin and T. Chen, *Adv. Protein Chem. Struct. Biol.*, 2018, **110**, 31–63.

23 D. R. Stroik, S. L. Yuen, K. A. Janicek, T. M. Schaaf, J. Li, D. K. Ceholski, R. J. Hajjar, R. L. Cornea and D. D. Thomas, *Sci. Rep.*, 2018, **8**, 12560.

24 Q. Wang, K. Nchimi Nono, M. Syrjänpää, L. J. Charbonnière, J. Hovinen and H. Härmä, *Inorg. Chem.*, 2013, **52**, 8461–8466.

25 U. Cho and J. K. Chen, *Cell Chem. Biol.*, 2020, **27**, 921–936.

26 G. Mathis and H. Bazin, Lanthanide Luminescence, *Springer Series on Fluorescence*, 2010, ch. 7, pp. 47–88.

27 V. Mukkala, M. Helenius, I. Hemmilä, J. Kankare and H. Takalo, *Helv. Chim. Acta*, 1993, **76**, 1361–1378.
28 T. Nishioka, J. Yuan, Y. Yamamoto, K. Sumitomo, Z. Wang, K. Hashino, C. Hosoya, K. Ikawa, G. Wang and K. Matsumoto, *Inorg. Chem.*, 2006, **45**, 4088–4096.
29 W. Li, M. J. Moore, N. Vasilieva, J. Sui, S. K. Wong, M. A. Berne, M. Somasundaran, J. L. Sullivan, K. Luzuriaga, T. C. Greenough, H. Choe and M. Farzan, *Nature*, 2003, **426**, 450–454.
30 X. Chen, R. Li, Z. Pan, C. Qian, Y. Yang, R. You, J. Zhao, P. Liu, L. Gao, Z. Li, Q. Huang, L. Xu, J. Tang, Q. Tian, W. Yao, L. Hu, X. Yan, X. Zhou, Y. Wu, K. Deng, Z. Zhang, Z. Qian, Y. Chen and L. Ye, *Cell. Mol. Immunol.*, 2020, **17**, 647–649.
31 A. E. Sauer-Eriksson, G. J. Kleywegt, M. Uhlén and T. A. Jones, *Structure*, 1995, **3**, 265–278.
32 M. Nosrati, S. Solbak, O. Nordesjö, M. Nissbeck, D. F. A. R. Dourado, K. G. Andersson, M. R. Housaindokht, J. Löfblom, A. Virtanen, U. H. Danielson and S. C. Flores, *Protein Eng., Des. Sel.*, 2017, **30**, 593–601.
33 W. L. DeLano, M. H. Ultsch, A. M. de Vos and J. A. Wells, *Science*, 2000, **287**, 1279–1283.
34 S. H. Ha, S. Y. Kim and J. E. Ferrell, *Cell Rep.*, 2016, **16**, 2047.
35 J. Xiang, L. Katz, P. L. Winokur, A. Chaudhary, B. Digmann, R. Bradford, S. Rashid, S. Ghosh, A. Robertson, J. Menetski, M. Xu, P. Gao, C. Z. Chen, T. Lee, B. Poelaert, R. T. Eastman, M. D. Hall and J. T. Stapleton, *J. Immunol. Methods*, 2024, **530**, 113698.
36 W. A. Haynes, K. Kamath, J. Bozekowski, E. Baum-Jones, M. Campbell, A. Casanovas-Massana, P. S. Daugherty, C. S. Dela Cruz, A. Dhal, S. F. Farhadian, L. Fitzgibbons, J. Fournier, M. Jhatro, G. Jordan, J. Klein, C. Lucas, D. Kessler, L. L. Luchsinger, B. Martinez, M. Catherine Muenker, L. Pischel, J. Reifert, J. R. Sawyer, R. Waitz, E. A. Wunder, M. Zhang, K. Anastasio, M. H. Askenase, N. C. Balkcom, M. Batsu, S. Bermejo, K. Brower, M. L. Bucklin, S. Cahill, Y. Cao, M. Chiorazzi, C. J. Chun, R. Datta, G. DeIuliis, C. E. Dorgay, R. Earnest, J. Fournier, B. Geng, R. Handoko, W. Khoury-Hanold, R. Herbst, L. Knaggs, M. Kuang, S. Lapidus, Z. Lin, P. Lu, T. Mao, A. Martin, I. Matos, D. McDonald, M. Minasyan, A. J. Moore, N. Naushad, A. Nelson, J. Nouws, A. Nunez, H.-J. Park, X. Peng, A. J. Robertson, T. Rice, K.-A. Rose, W. Schulz, L. Sewanan, L. Sharma, D. Shepard, J. Silva, M. Simonov, M. Smolgovsky, N. Sonnert, A. Srivathsan, Y. Strong, C. Todeasa, J. Valdez, S. Velazquez, P. Vijayakumar, E. B. White, A. Zhao, A. Iwasaki, A. Ko and J. C. Shon, *Commun. Biol.*, 2021, **4**, 1317.
37 Md. A. Mahmud, L. H. Xu, A. Usatinsky, C. C. dos Santos, D. J. Little, S. S. H. Tsai and D. G. Rackus, *Anal. Chem.*, 2024, **96**, 11751–11759.
38 P. Brodin and M. M. Davis, *Nat. Rev. Immunol.*, 2017, **17**, 21–29.
39 J. J. Morales-Núñez, J. F. Muñoz-Valle, P. C. Torres-Hernández and J. Hernández-Bello, *Vaccines*, 2021, **9**, 1376.
40 N. Y.-L. Pang, A. S.-R. Pang, V. T. Chow and D.-Y. Wang, *Mil. Med. Res.*, 2021, **8**, 47.
41 H. Yue, R. P. Nowak, D. Overwijn, N. C. Payne, S. Fischinger, C. Atyeo, E. C. Lam, K. St. Denis, L. K. Brais, Y. Konishi, R. Sklavenitis-Pistofidis, L. R. Baden, E. J. Nilles, E. W. Karlson, X. G. Yu, J. Z. Li, A. E. Woolley, I. M. Ghobrial, J. A. Meyerhardt, A. B. Balazs, G. Alter, R. Mazitschek and E. S. Fischer, *Cells Rep. Methods*, 2023, **3**, 100421.